Journal of Rare Earths 43 (2025) 1373–1381

Contents lists available at ScienceDirect

Journal of Rare Earths

journal homepage: http://www.journals.elsevier.com/journal-of-rare-earths

Trichromatic color tuning strategy for emission of heterometallic Eu^{III}/Tb^{III} coordination polymers with triazolyl-substituted 4-methyl-phenoxo ligand☆

Juliana Perez-Obando [a], Jorge Manzur [a], Pablo Fuentealba [a, **], Jeannette Morales [a], Andrés Vega [b], Ricardo Costa de Santana [c], Albano N. Carneiro Neto [d, *], Evgenia Spodine [a, ***]

[a] Faculty of Chemical and Pharmaceutical Sciences, University of Chile, Olivos 1007, 8380544, Santiago, Chile
[b] Chemistry Department, University Andrés Bello, Av. República 498, 8370011, Santiago, Chile
[c] Physics Institute, Federal University of Goiás, Campus Samambaia, 74690-900, Goiânia, GO, Brazil
[d] Physics Department and CICECO – Aveiro Institute of Materials, University of Aveiro, 3810-193, Aveiro, Portugal

ARTICLE INFO

Article history:
Received 26 February 2024
Received in revised form
27 May 2024
Accepted 26 June 2024
Available online 28 June 2024

Keywords:
Europium(III)
Terbium(III)
Heterometallic coordination polymers
Trichromatic strategy
Rare earths

ABSTRACT

This study presents the microwave-assisted synthesis and characterization of a series of heterometallic coordination polymers (HMCPs) with a 4-methyl-2,6-di[(1H-1,2,4-triazol-1-yl)]phenoxo ligand with varying Eu^{III}/Tb^{III} ratios. Single crystal X-ray diffraction reveals a double-chain structure bridged by triazolyl groups. Powder X-ray diffraction confirms the isostructural nature of the synthesized HMCPs. The photophysical properties depend on lanthanide ion concentration and excitation wavelength, leading to a color shift from green to blue as the proportion of Tb^{III} decreases and Eu^{III} increases. White light generation is achieved in the 8/2 Eu^{III}/Tb^{III} HMCP (CIE: 0.293, 0.326) under 335 nm excitation. The study suggests energy transfer from Tb^{III} to Eu^{III}, but both experimental and theoretical calculations indicate that this transfer is orders of magnitude lower than the sensitization through ligand states.

1. Introduction

Nowadays, inorganic phosphors such as aluminate, silicate and oxynitride are usually the most used inorganic materials in the manufacture of phosphor-converted white light-emitting diodes (pc-WLEDs); however, they have significant drawbacks. As each one of the components is monochromatic, there is a need to mix several emitting phosphors of different colors to obtain white light with color rendering, which can lead to phase separation and instability during application.[1] In this sense, an innovative approach is the incorporation of lanthanide ions in coordination polymers, by the synthesis of single-phase materials with cooperative optical properties, which allows the generation of white light in the solid state.[2–6] Special interest has been placed in the synthesis of coordination polymers for luminescent applications, thanks to the thermal and photochemical stability that they present.[7,8] Besides, due to their single-phase nature, there is no possibility of phase separation. The importance of studying new optical systems that generate white light lies in their varied and important applications for LED lighting devices[9–13] and sensing.[14]

Solid-state white light can be generated by combining the emission of two colors (blue and yellow), three colors (blue, red, and green), or four colors (blue, cyan, green, and red). The trichromatic alternative is convenient since it presents a good balance between the luminous efficiency of dichromatic sources

☆ **Foundation item:** Project supported by Fondo Nacional de Desarrollo Científico y Tecnológico, FONDECYT (1200033), the National Doctoral Scholarship (21192195), Chile, Conselho Nacional de Desenvolvimento Científico e Tecnológico (CNPq, 427164/2018–4 and 310307/2021–0) and Fundação de Amparo à Pesquisa do Estado de Goiás (FAPEG), Brazil, and developed within the scope of the project CICECO-Aveiro Institute of Materials (UIDB/50011/2020, UIDP/50011/2020, LA/P/0006/2020) and LogicALL (PTDC/CTMCTM/0340/2021) financed through the FCT-Foundation for Science and Technology/Ministry of Education (PIDDAC-Central Government Investment and Development Expenditure Program), Portugal.

* Corresponding author.
** Corresponding author.
*** Corresponding author.
E-mail addresses: pfuentealbacastro@ciq.uchile.cl (P. Fuentealba), albanoneto@ua.pt (A.N. Carneiro Neto), espodine@ciq.uchile.cl (E. Spodine).

https://doi.org/10.1016/j.jre.2024.06.036

and the great color reproduction capacity of tetrachromatic ones.[15] In this sense, heterometallic coordination polymers (HMCPs) offer a promising alternative to generate white light emission through the incorporation of lanthanide ions of Eu^{III} (red emission) and Tb^{III} (green emission) together with organic ligands that contribute emission in the blue color region.[16–18] In addition, the organic ligands make possible the enhancement of the particular luminescent properties of the Ln^{III} ions by luminescence sensitization or "antenna effect".[19–21]

The interest in synthesizing light emitting systems by incorporating Eu^{III} and Tb^{III} ions into HMCPs also lies in the control of the modulation of the emitted color depending on the molar ratio of each lanthanide ion into the coordination polymeric network.[22–25] For example, Liu et al.[22] synthesized a series of Tb^{III}/Eu^{III} isostructural HMCPs (L-Tb_xEu_{1-x}) with L: 4-cyano-3-methylbenzoic acid, which when irradiated with 365 nm wavelength exhibited continuous luminescent color changes: from green to yellow, orange and red as the proportion of Tb^{III} was decreased while that of Eu^{III} increased.

Moreover, the modulation of the color in coordination polymers with Eu^{III} and Tb^{III} ions reported in the literature shows that the changes in the CIE color coordinates depend not only on the molar ratio of the Ln^{III} ions, but also on the excitation wavelength.[4,26] Thus, Kang et al.[26] reported the synthesis and photophysical properties of a series of fluorescent Eu–Tb (btc) polymers (1,2,4-H_3btc: 1,2,4-benzenetricarboxylic acid). When $Eu_{0.5}Tb_1(btc)_{1.5}$ was excited with a wavelength of 375 nm, white light with CIE coordinates of (0.334, 0.311) was obtained. On the other hand, when they modulated the Eu^{III}/Tb^{III} molar ratio in the $Eu_xTb_1(btc)_{1+x}$ polymers ($x = 0$, 0.2, 0.3, 0.5, 1), it was possible to observe that by increasing the Eu^{III} ratio under excitation wavelength at 375 nm, the green emission from the Tb^{III} center decreased, and the emission color of the polymers changed from green to white, and finally to red with a higher proportion of Eu^{III}.

The present investigation is related to the synthesis and characterization of a new series of HMCPs with different molar ratios of Eu^{III} and Tb^{III} ions, with 4-methyl-2,6-di[(1H-1,2,4-triazol-1-yl)] phenol ($L^{Me}Tr$). The influence of the Eu^{III}/Tb^{III} molar ratio on the generation of white light and the dependence on the excitation wavelength is reported. Besides, theoretical calculations contributed to the understanding of the energy transfer processes involved in the emission of the HMCPs.

2. Experimental

2.1. Synthesis

All reagents were used without previous purification. A Microwave Monowave 200 Anton Parr equipment was used to prepare the heterometallic coordination polymers.

The synthesis of the $L^{Me}Tr$ ligand was previously described.[27,28] To synthesize the Eu^{III} and Tb^{III} heterometallic complexes with the $L^{Me}Tr$ ligand, 0.5 mmol of the $L^{Me}Tr$ ligand was dissolved in 10 mL of acetonitrile. Subsequently, 0.5 mmol triethylamine (TEA) was added in order to deprotonate the phenol group of the ligand. Solutions with "x mmol" of $Eu(NO_3)_3{\cdot}5H_2O$ and "0.5–x mmol" of $Tb(NO_3)_3{\cdot}5H_2O$ were prepared using 5 mL of acetonitrile; it was necessary to sonicate for 5 min in order to obtain complete dissolution. Afterwards, each solution (Eu^{III}/Tb^{III}: 1/9, 2/8, 3/7, 4/6, 5/5, 6/4, 7/3, 8/2, 9/1) was mixed with a solution of the deprotonated ligand. The reaction mixture was heated at 100 °C for 15 min, using microwave radiation. The reaction solution was filtered, and after a slow evaporation of the solvent, the HMCPs were obtained as microcrystalline solids. These were separated and dried in a vacuum desiccator.

All HMCPs presented the same vibrational profile, as evidenced by FTIR spectra (Fig. S1). FTIR: Eu^{III}/Tb^{III}-$L^{Me}Tr$: 3452 cm^{-1} (ν_{O-H}); 3119 cm^{-1} (ν_{C-H}, triazole); 2954 cm^{-1} (ν_{CH}, methyl); 1631, 1522, 1503 cm^{-1} ($\nu_{C=C,\ C=N}$, aromatic); 1470, 1297 cm^{-1} (ν_{NO_3}); 1137 cm^{-1} (ν_{C-O}). The metal composition of the HMCPs was established by SEM-EDXS, giving the expected Eu^{III}/Tb^{III} ratios. The ratios were also confirmed by atomic absorption (Table S1).

2.2. Measurements

Fourier transform infrared (FTIR) spectra were recorded in the 4000–500 cm^{-1} range, on a Spectrum Two-Perkin Elmer spectrophotometer, coupled with an attenuated total reflectance accessory from Pike Instruments. Single crystal X-ray diffraction was recorded on a SMART-APEX II CCD diffractometer at room temperature. Powder X-ray diffraction analyses were performed at room temperature using a Bruker D-8 Advance equipment, with Cu Kα1 radiation. Scanning electron microscopy analyses were executed using a Thermo Fisher Scientific high-resolution scanning electron microscope (SEM, Inspect F50, FEI), coupled to a Thermo Fisher Scientific Ultradry Pathfinder Alpine 129 eV EDX detector. A Cressington TEDPELLA sputter coater, model 108 and a non-conductive film coater were used for coating the films. The atomic absorption analyses were done with a PerkinElmer, pinAAcle 900F spectrophotometer. Photoluminescence (PL) solid-state emission spectra were measured using a Horiba-Jobin Yvon spectrofluorometer, model Fluorolog-3 (FL3-221), under excitation with a 450 W Xe arc lamp, and a Horiba PPD-850 ps photon detector in the UV-VIS region. The emission decay curves for Tb^{III} and Eu^{III} heterometallic compounds were obtained using Xe pulsed lamp, and they were properly fitted with a bi-exponential function. The average emission lifetime ($\bar{\tau}$) was calculated from Eq. (S1).

The CIE 1931 (Commission International d'Eclairage) coordinates (x, y) and color diagram were calculated from the emission spectra.[29] The correlated color temperature (CCT) was calculated using McCamy's[30] polynomial formula.

$$CCT = -437n^3 + 3601n^2 - 6861n + 5514.31 \quad (1)$$

where $n = (x - x_e)/(y - y_e)$, x and y being the color coordinates, and $x_e = 0.3320$ and $y_e = 0.1858$ being the chromatic epicenter. The CCT is related to the temperature at which a blackbody must be heated to exhibit a warm-toned or a cold-toned white light. Between 2500 and 3500 K the white light is warm-toned, with yellow and orange color components. Above 4500–6500 K CCT values the white light is cold-toned, with cyan and blue color components.

3. Theoretical

The energy transfer rates between a pair of lanthanide ions can be calculated using the Kushida-Malta model.[31–33] This model incorporates various mechanisms, including dipole–dipole (W_{d-d}, Eq. (S2)), dipole–quadrupole (W_{d-q}, Eq. (S3)), quadrupole–quadrupole (W_{q-q}, Eq. (S4)), exchange (W_{ex}, Eq. (S5)), and magnetic dipole–magnetic dipole (W_{md-md}, Eq. (S6)) mechanisms.[31–35] The mechanisms W_{q-q}, W_{ex}, and W_{md-md} operate independently of the Judd–Ofelt parameters (Ω_λ). The ρ_{f-f} in Eq. (S5) represents the overlap integral between the 4f subshells of the donor (D) and acceptor (A) lanthanide ions. These values were computed using density functional theory and the ρ_{f-f} values as a function of donor–acceptor distance (Tb–Eu distance, R) can be found in the literature.[36] Non-radiative energy transfer involving magnetic dipole interactions in inorganic solids was addressed in the early 1950s by Dexter.[37] In the 1990s, these interactions found application in the energy transfer between lanthanide ions in

inorganic crystals, as discussed by Tanner et al.[38,39] For further details on the quantities involved in the Ln-to-Ln energy transfer rates (Eqs. (S2)–(S6)), see section 4 of the Supplementary Information.

The spectral overlap factor, (F, Eq. (S7)) for a specific pathway should be multiplied by the energy barrier factor $\exp(\delta/k_BT)$ if δ (the energy difference between donor and acceptor transitions, $\delta = E_D - E_A$) is negative, where k_B is the Boltzmann constant and T is the temperature. Additionally, depending on the energy transfer pathway, the population of the starting acceptor level should be considered. For example, the population of the Eu^{III} $^7F_1$ is thermally populated from the ground $^7F_0$ following a Boltzmann statistic. Thus, at room temperature, the population of the $^7F_1$ can reach 33%, while the $^7F_0$ stays at 65%.[40] In this context, we will consider these populations as numerical factors (P) multiplying all the mechanisms, forming the pathway energy transfer rate $W(p)$:

$$W(p) = \left[W_{d-d}(p) + W_{d-q}(p) + W_{q-q}(p) + W_{ex}(p) + W_{md-md}(p)\right] \cdot P \quad (2)$$

with $P = 0.33$ or 0.65 if the pathway involves the $^7F_1$ or $^7F_0$ of the Eu^{III} as the initial level of the $Tb^{III} \rightarrow Eu^{III}$ energy transfer process. For instance, the rate obtained for the pathway Tb^{III} [$^5D_4 \rightarrow {}^7F_6$] → Eu^{III} [$^7F_0 \rightarrow {}^5D_2$] will be multiplied by 0.65, while the pathway Tb^{III} [$^5D_4 \rightarrow {}^7F_6$] → Eu^{III} [$^7F_1 \rightarrow {}^5D_2$] will be multiplied by 0.33. When all rates are obtained for each pathway, the total energy transfer rate is calculated as the sum of all pathways: $W_{total} = \sum W(p)$.

4. Results and discussion

4.1. Structural and morphological description

Crystals suitable for X-ray diffraction were only obtained for the 4/6 Eu^{III}/Tb^{III} HMCP and used for the structure determination. As a unique metal-ion site is present in the asymmetric unit, a mixed Eu^{III}/Tb^{III} composition was introduced into the last stages of refinement, including two equivalent positions for both cations whose occupancies were forced to add one. These were refined and set constant to 0.40 and 0.60 for Eu^{III} and Tb^{III} respectively for the final refinement (Fig. S2 and Table S2–S4). Fig. 1(a) shows a scheme of the first coordination sphere of the Ln^{III} ions, while structural details are given in Fig. S2, and Fig. 1(b) displays the double chain that extends along the crystallographic a-axis.

The crystalline structure of the HMCPs is the same for all Eu^{III}/Tb^{III} compounds, as evidenced by powder X-ray diffraction (PXRD). Fig. S3 depicts the corresponding powder diffractograms, where it becomes evident that the position of the diffraction peaks does not vary from sample to sample. Besides, the experimental PXRD patterns of HMCPs coincide with the simulated PXRD pattern of the 4/6 Eu^{III}/Tb^{III} HMCP and the experimental PXRD pattern of the Eu^{III} homometallic CP analogue, whose structure was previously reported.[41] This indicates that the synthesized HMCPs correspond to a family of isostructural compounds. This isostructural character is frequently observed in coordination polymers when incorporating different lanthanide centers.[5,22,42]

The SEM-EDXS permitted the determination of the relative Eu^{III} and Tb^{III} molar ratios of the resulting HMCPs (Table S5). The obtained percentage of the two lanthanide ions are close to the used molar ratio during the preparation procedures. Moreover, mapping analyses of the Eu^{III} and Tb^{III} ions showed that the distribution of the lanthanide ions is homogeneous (Fig. 2).

An enlarged SEM image was recorded for the 8/2 polymer, with a magnification of 5000×, the image presents a visualization scale of 10 μm. This micrograph showed that the sample was composed of stacked particles, which can be described as blocks of different micrometric lengths (Fig. S4).

4.2. Solid-state photoluminescence

Fig. 3(a) shows selected excitation spectra for the HMCPs monitoring the 546 nm emission band of Tb^{III} in comparison with the homonuclear CP. The spectra are dominated by intense broadband from 300 to 340 nm corresponding to the absorption of the ligand; expansion of the spectra permits the observation of several bands at 348, 354, 359, 366, and 379 nm, which can be assigned to Tb^{III} transitions (Fig. 3). The intensity of these bands decreases as the composition of Tb^{III} in the HMCP declines, but the profile of the spectra is retained. On the other hand, Fig. 3(c and d) depict selected excitation spectra monitoring the 615 nm emission of Eu^{III}, where a significant variation of the profile of the spectra is observed. For the 1/9 and 2/8 HMCPs, the profile is similar to that of the Tb^{III} spectrum, while for the HMCPs with a higher proportion of Eu^{III} the spectra change drastically showing a band centered at *ca.* 335 nm. The corresponding spectra of the 9/1 HMCP are given in

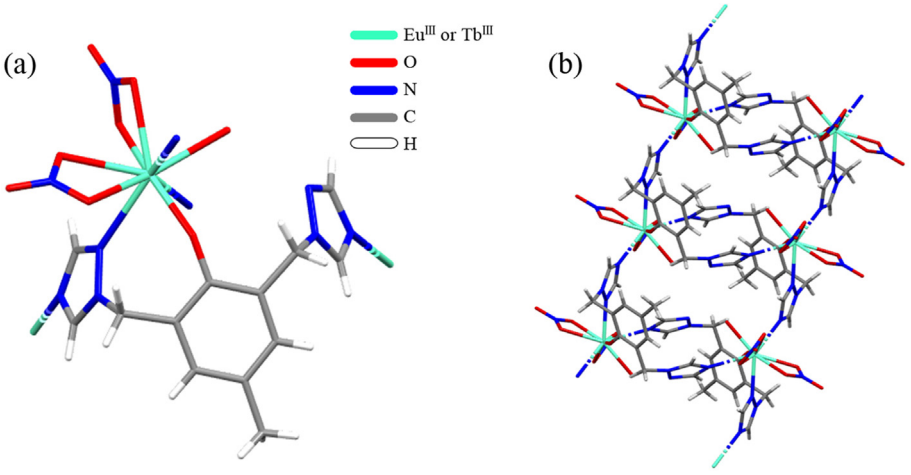

Fig. 1. (a) First coordination sphere of lanthanide ions for the 4/6 Eu^{III}/Tb^{III} HMCP; (b) Extended structure of the HMCP. Dotted lines represent bonds between nitrogen donor atoms of triazole units and Ln^{III} ions, which promote the formation of the chains.

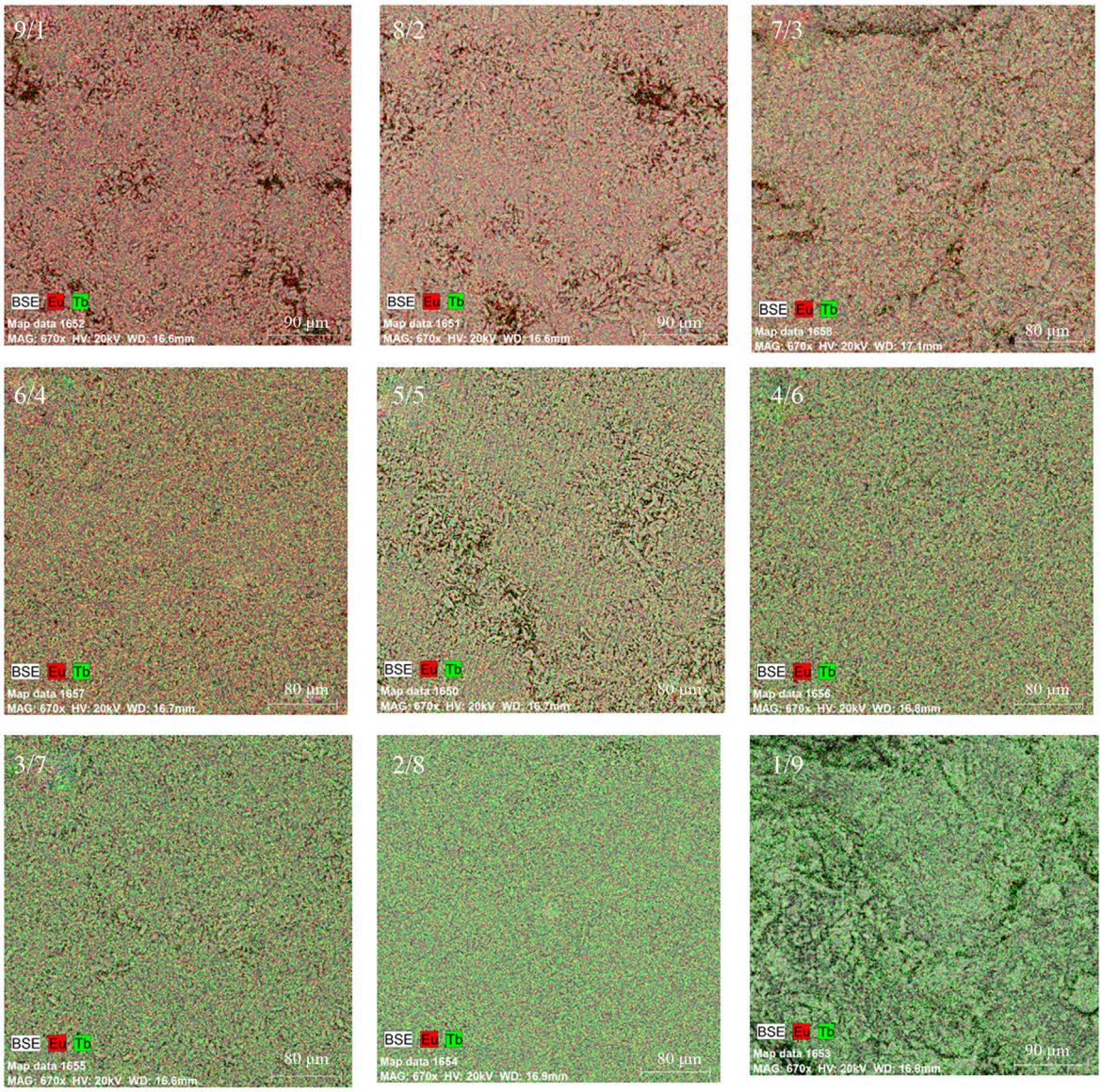

Fig. 2. SEM-EDXS mapping images of HMCPs.

the Supplementary Information (Fig. S5). All spectra present the characteristic 395 nm band due to the Eu^{III} $^7F_0 \rightarrow {}^5L_6$ transition.

For the entire series of HMCPs, the corresponding solid-state photoluminescence study was performed using different excitation wavelengths: 325, 330, and 335 nm, unless otherwise stated. Fig. S6 depicts the emission spectra for the 1/9 and 9/1 Eu^{III}/Tb^{III} HMCPs at the mentioned excitation wavelengths, and their corresponding CIE diagram. It becomes evident that for a high proportion of Tb^{III} in the HMCP the spectra are dominated by the green $^5D_4 \rightarrow {}^7F_5$ transition (Fig. S6(a)). On the other hand, for a high proportion of Eu^{III} the blue emission of the $L^{Me}Tr$ ligand dominates the spectra (Fig. S6(c)). This can be attributed to the high concentration of the Eu^{III} ion, where the antenna effect is not efficient, as compared to that observed in the case when an excess of Tb^{III} is present as in the 1/9 HMCP.

As the ligand sensitizes more efficiently the Tb^{III} than Eu^{III} center, the blue emission of the ligand for the 1/9 HMCP is almost absent (Fig. S6(a)); the opposite effect is observed for the 9/1 HMCP where the blue contribution is significantly enhanced (Fig. S6(c)). Furthermore, the $^5D_4 \rightarrow {}^7F_5$ emission at 546 nm from the Tb^{III} cation decreases for the 1/9 HMCP as the excitation wavelength increases, and a similar behavior is observed for the 9/1 HMCP.

The only pure bands in the emission spectra for the HMCPs are the $^5D_4 \rightarrow {}^7F_6$ at 490 nm and $^5D_4 \rightarrow {}^7F_5$ at 546 nm for the Tb^{III} centers. Moreover, the emission bands between 575 and 630 nm are composed by the emission of the Eu^{III} and Tb^{III}. Fig. S7 depicts these combined emissions for all the synthetized HMCPs. In the 575–591 nm region, the emission spectra contain the contributions of luminescence from $^5D_0 \rightarrow {}^7F_{0,1}$ transitions of Eu^{III} and the $^5D_4 \rightarrow {}^7F_4$ transition of Tb^{III}. Besides, in the 615–621 nm region, the emission spectra enclose the contribution of luminescence from the $^5D_0 \rightarrow {}^7F_2$ transition of Eu^{III} and the $^5D_4 \rightarrow {}^7F_3$ transition of Tb^{III}. The observed shift in the position of the emission bands and the variation of the intensity are a consequence of the mentioned contributions. The contribution of the 583 nm band should be mainly the $^5D_4 \rightarrow {}^7F_4$ emission from Tb^{III}.

CIE chromaticity diagrams for all synthesized HMCPs are shown in Fig. 4 and the corresponding emission spectra are included in the Supplementary Information (Figs. S8–S13). For each analyzed wavelength, the HMCPs with a high proportion of Tb^{III} (1/9, 2/8, and

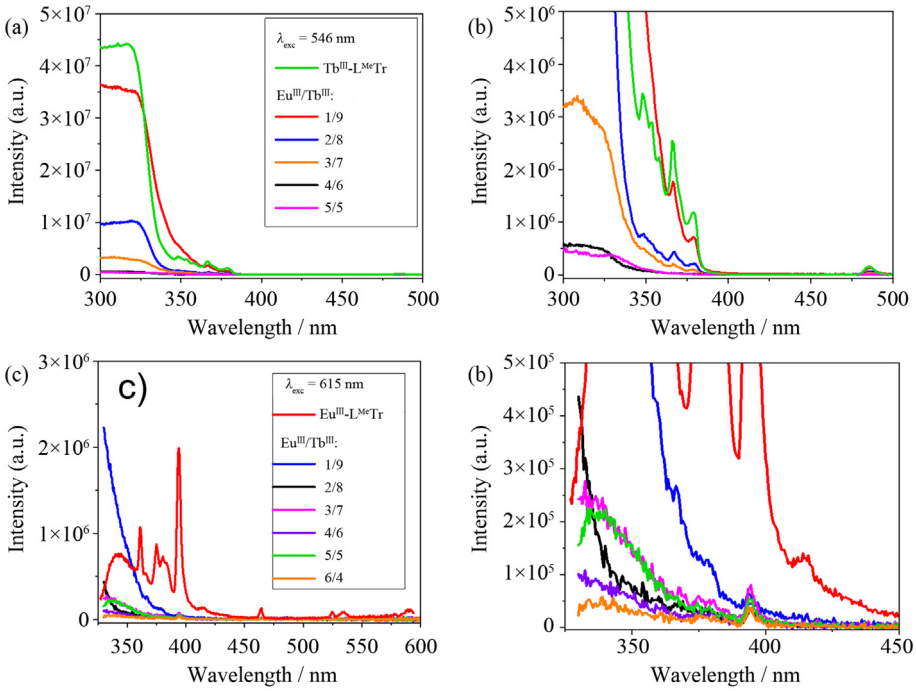

Fig. 3. Excitation spectra of selected HMCPs monitoring at 546 nm (Tb^{III}) (a) and 615 nm (Eu^{III}) (c) emissions, with respective enlargements in the 300–500 nm (b) and 325–450 nm (d) regions.

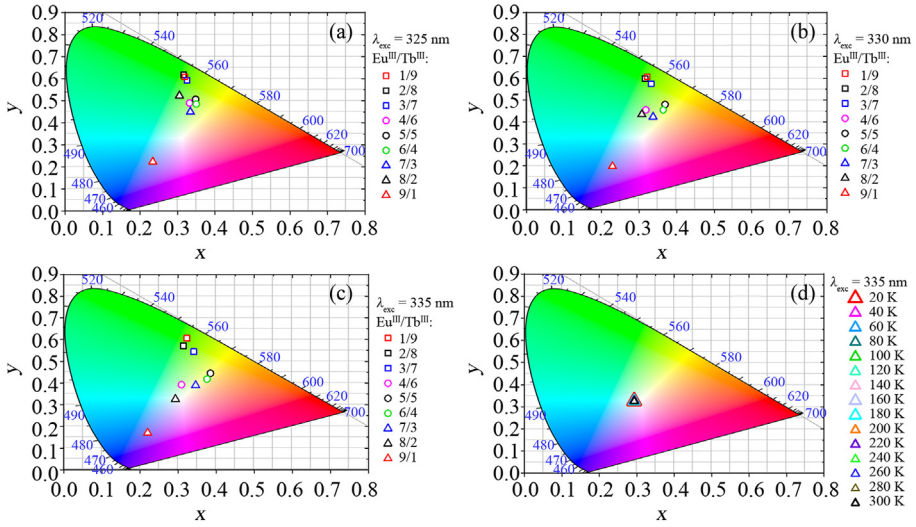

Fig. 4. CIE chromaticity coordinates for HMCPs using different excitation wavelengths. (a) λ_{exc} = 325 nm; (b) λ_{exc} = 330 nm; (c) λ_{exc} = 335 nm. (d) Temperature dependence of the CIE chromaticity coordinates for the 8/2 Eu^{III}/Tb^{III} HMCP emission when excited at 335 nm.

3/7) emit in the green color range, while the HMCP with a high proportion of Eu^{III} (9/1) emits in the blue color range. For comparison purposes, the emission spectra and CIE chromaticity diagrams for the homometallic samples are shown in Fig. S14.[41] It is clear that the CIE coordinates of the HMCPs systematically fall between those of the homometallic samples. This also suggests that the energy transfer process is dominated by intramolecular interactions (ligand-to-Ln energy transfer rates), rather than the Tb^{III}-to-Eu^{III} energy transfer process. This is further confirmed by the analysis of the Tb^{III} $^5D_4$ emission lifetimes and theoretical calculations.

Fig. 4(c) shows that the 8/2 Eu^{III}/Tb^{III} HMCP, when excited at 335 nm, emits close to the white light region with CIE chromaticity coordinates of (0.293, 0.326) (0.333, 0.333 for white light). The CIE chromaticity coordinates do not present thermal dependence as shown in Fig. 4(d). These color coordinates correspond to a 7460 K CCT, indicating that this polymer is a cold-toned white light emitter.[43] The 8/2 Eu^{III}/Tb^{III} HMCP can emit white light because the high Eu^{III} proportion allows the ligand to emit blue light in a suitable proportion with that of the red and green emission of Eu^{III} and Tb^{III} respectively, creating an appropriate trichromatic system for white light emission.

However, not only the appropriate Eu^{III}/Tb^{III} ratio is important to achieve white light emission, but the choice of the excitation wavelength is also significant. Thus, the 8/2 Eu^{III}/Tb^{III} HMCP can emit white light only when excited at 335 nm. Fig. 5(a) (inset) depicts that for this excitation wavelength, the spectrum presents a greater ligand emission in the blue region (380–475 nm) with a moderate emission from the Eu^{III} and Tb^{III} centers. The moderate emission from Eu^{III} and Tb^{III} centers makes the blue emission of the ligand more relevant, which influences the CIE coordinates of the emitted light permitting the generation of white light. On the other hand, when a lower energy excitation wavelength is used (367 nm) the CIE color coordinates correspond to the blue region (0.231, 0.207) (Fig. 5(b)); this is due to the low emission of Tb^{III} at this excitation wavelength (Fig. 5(a); yellow curve).

In order to have a better insight into the processes involved in the light emission of the studied HMCPs, the compounds were irradiated with lower energy (λ_{exc} = 395 nm). Fig. S15 shows the corresponding emission spectra for selected HMCPs (Eu^{III}/Tb^{III}: 2/8, 3/7, and 4/6), where it is possible to visualize a band at 546 nm for the 2/8 and 3/7 (Eu^{III}/Tb^{III}) HMCPs, which is assigned to the Tb^{III} $^5D_4 \rightarrow {}^7F_5$ emission. At lower Tb^{III} concentrations this band is too weak to be detected. Even though the maximum excitation wavelength for Tb^{III} emission ranges from 300 to 340 nm as can be observed in the excitation spectra (Fig. 3(b) and Fig. S5), the same spectra show a tail to lower energies, which permits the excitation of the Tb^{III} centers.

4.3. Tb^{III}-to-Eu^{III} energy transfer rates

Since we are dealing with a heterometallic system, energy transfer between the two centers (Tb^{III} and Eu^{III}) may occur. One strategy to experimentally determine the energy transfer rates from Tb^{III} to Eu^{III} is analyzing the change of the emission lifetimes of the Tb^{III} $^5D_4$ (donor) in the presence and the absence of the Eu^{III} (acceptor), τ_{DA} and τ_D respectively. Therefore, the decay processes of the studied HMCPs were undertaken. The samples were excited at 325 nm at room temperature, using this wavelength to promote the excitation of the Tb^{III} centers by the antenna effect. The decay of the Tb^{III} emission at 546 nm was monitored in order to detect the energy transfer from this lanthanide ion to Eu^{III}. The corresponding decay curves and bi-exponential fitting are given as Supplementary Information (Fig. S16), and the obtained τ values are in Table 1. A lower value for Tb^{III} is evidenced as compared to that of the homometallic species (the reported τ value is 1020 μs (k = 0.98 × 10^3 s^{-1})), while the Eu^{III} has an increased lifetime.[41]

The decrease of the lifetime values for the decay of the Tb^{III} emission would be related to the depopulation of the Tb^{III} level as the energy transfer to Eu^{III} takes place. This phenomenon has been observed in different materials, containing Tb^{III} and Eu^{III}, and the energy transfer pathways have been described in literature.[33,40] For instance, Wei et al. analyzed energy transfer from Tb^{III} to Eu^{III} showing a thermal dependence of this phenomenon, which can be used in thermometry.[44] On the other hand, heterometallic Tb^{III}-Eu^{III} binuclear complexes were shown to present a direct Tb^{III} to Eu^{III} energy transfer.[45] Besides, theoretical calculations have shown that the Ln-to-Ln energy transfer process is only comparable with that of the ligand-to-Ln when short Ln–Ln distances are involved.[32,46,47]

Table 1
Values of average lifetimes ($\bar{\tau}$ in μs), Tb^{III}-Eu^{III} energy transfer rates (in s^{-1}), and efficiencies (%) according to the Eu^{III}/Tb^{III} relation for selected HMCPs samples.

Eu^{III}/Tb^{III} HMCPs	$\bar{\tau}$ (Eu^{III})	$\bar{\tau}$ (Tb^{III})	W_{exp}	η_{ET}
0/10	–	1020[a]	–	–
2/8	487	805	262	21
4/6	545	598	692	41
5/5	499	879	157	14
9/1	523	795	278	22
10/0	180[a]	-	–	–

[a] From Ref. 41.

The experimental energy transfer rate (W_{exp}) and the energy transfer efficiency (η_{ET}) can be calculated by[33,40,48]:

$$W_{exp} = \frac{1}{\tau_{DA}} - \frac{1}{\tau_D} \quad (3)$$

$$\eta_{ET} = 1 - \frac{\tau_{DA}}{\tau_D} \quad (4)$$

For example, the homometallic Tb^{III} coordination polymer lifetime is τ_D = 1020 μs [41] and the measured τ_{DA} value of 805 μs for the 2/8 (Eu^{III}/Tb^{III}) HMCP, consequently, we can estimate W_{exp} = 262 s^{-1} and η_{ET} = 21%. These values appear relatively low compared to those reported in the literature.[33,40] As a reference, heterometallic metal–organic frameworks (MOFs) containing Tb^{III} and Eu^{III} in different proportions have demonstrated W_{exp} values higher than 10^3 s^{-1} and η_{ET} values ranging from 72% to 92%.[40,49] The average lifetimes values, as well as the energy transfer rates and efficiencies, for selected HMCPs are given in Table 1.

The relatively low values of W_{exp} and η_{ET} for the HMCPs can be attributed to the considerable distance between Tb^{III} and Eu^{III} ions. According to the crystallographic structure, the shortest distance is 0.703 nm, which is considered large for an effective interaction between the two lanthanide ions.[46] For comparison, the shortest Tb^{III}–Eu^{III} distance in the dual-center $Tb_{0.94}Eu_{0.06}(bpy)_2(NO_3)_3$ coordination compound (bpy = 2,2′-bipyridine) is 0.77 nm, resulting in a similar order of magnitude for the Tb^{III}-Eu^{III} energy transfer rates (~10^2 s^{-1}).[46] Thus, we can conclude that the sensitization

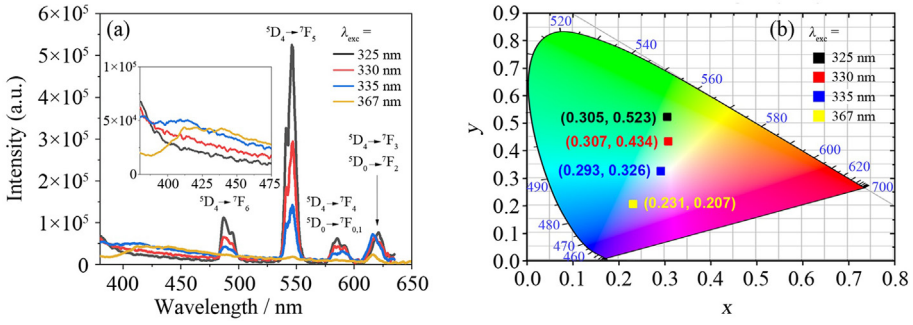

Fig. 5. (a) Emission spectra at room temperature of 8/2 Eu^{III}/Tb^{III} HMCP (black: λ_{exc} = 325 nm; red: λ_{exc} = 330 nm; blue: λ_{exc} = 335 nm; yellow: λ_{exc} = 367 nm). Inset: expanded spectra in the 350–475 nm region; (b) CIE chromaticity diagram.

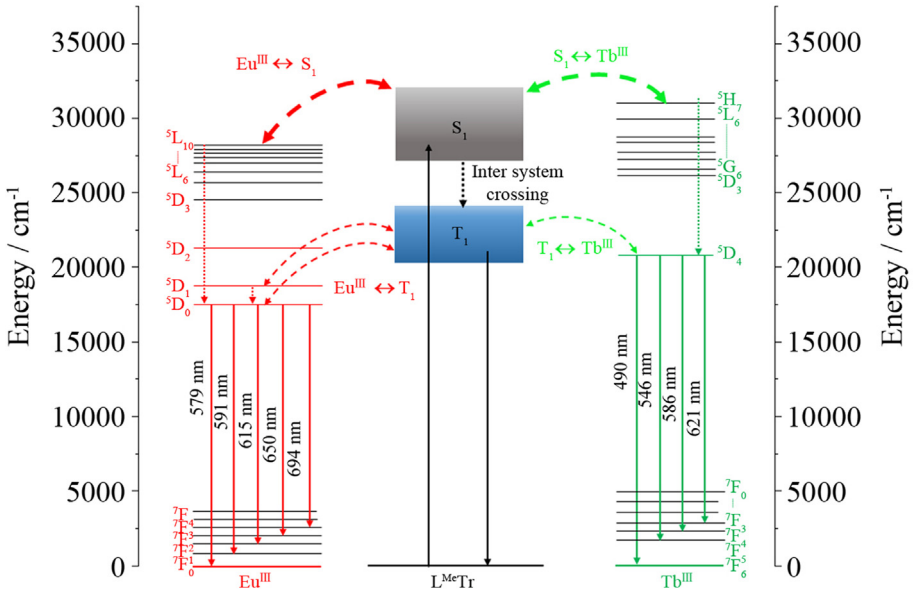

Fig. 6. Energy diagram for the sensitization processes of the HMCPs.

process in the studied HMCPs is mainly due to the energy transfer rates from the ligands to the Ln^{III}, which exhibit orders of magnitude higher values, especially from the singlet state.[41]

The theoretically calculated energy transfer (W_{total} = 610 s^{-1}, Table S6) aligns with the experimental data range obtained through Eq. (3) (values in Table 1). It is important to highlight that, considering the Tb^{III}-Eu^{III} energy transfer, the main energy transfer pathway, involving the nonradiative energy transfer from the donor Tb^{III} [$^5D_4 \rightarrow {}^7F_5$] to the acceptor Eu^{III} [$^7F_1 \rightarrow {}^5D_1$] transitions (pathway 9 in Table S6), has a major contribution from the quadrupole–quadrupole mechanism (W_{q-q}, Eq. (S4)), accounting for almost the entirety of W_{total}. Even with the presence of Tb^{III}-Eu^{III} energy transfer, these rates are orders of magnitude lower than the ligand-Tb^{III} and ligand-Eu^{III} interactions, as previously calculated for the homometallic analogues.[41] For instance, the energy transfer via the singlet state (S_1) to Eu^{III} was estimated to be in the order of 2.9×10^7 s^{-1}, representing a factor of more than 10000 times higher than the Tb^{III}-Eu^{III} rate. In this context, we can confirm that the sensitization process of the Eu^{III}/Tb^{III} heterometallic coordination polymer is primarily driven by energy transfer processes from ligands to the Ln^{III} rather than Tb^{III}-Eu^{III} energy transfer.

Therefore, taking into consideration that the photophysical process is barely dependent on the Ln^{III}-Ln^{III} energy transfer interaction, the sensitization process depicted in Fig. 6 can be proposed for the heterometallic coordination polymers. The sensitization process starts with ligand absorption, then, the energy transfer occurs between ligand (S_1 and T_1) and Ln^{III} excited states. The energy transfer includes forward and backward rates as detailed in Ref. 41, emphasizing the primary contribution from the S_1 state, which is represented by thicker arrows in Fig. 6. This elucidates the color tuneability observed with different excitation wavelengths.

The single-phase white light emitters reported in the literature, which use the trichromatic strategy of blue/red/green with different Eu^{III}/Tb^{III} ratios of the HMCPs, normally give a tunable emission from red to green. In this work, the reported Eu^{III}/Tb^{III} HMCPs were shown to achieve a tunable emission from blue to green at the used excitation wavelengths (335–325 nm) without reaching the red color. Furthermore, the 8/2 Eu^{III}/Tb^{III} HMCP generated a tunable emission from blue to white and finally to green, by modulating the excitation wavelength.

5. Conclusions

The synthesis and characterization of an isostructural series of heterometallic coordination polymers with Eu^{III} and Tb^{III} and 4-methyl-2,6-di[(1H-1,2,4-triazol-1-yl)]phenoxo as a ligand was successfully achieved by an efficient microwave-assisted reaction. The emission properties of the HMCPs series depend on the ratio of the lanthanide ions and the excitation wavelength. Interestingly, the emission of the studied HMCPs varies from green to blue; for high Eu^{III} content red emission is not obtained, due to the poor sensitization of this cation by the ligand. The 8/2 Eu^{III}/Tb^{III} HMCP, when excited at 335 nm, shows an emission that is close to the white light region with CIE coordinates (0.293, 0.326), which are temperature invariant. This emission has a CCT value of 7460 K CCT, indicating that the 8/2 Eu^{III}/Tb^{III} HMCP is a cold-toned white light emitter.

Regarding the sensitization process, the estimated low values of experimental energy transfer rates (W_{exp}) and efficiency (η_{ET}) in HMCPs are attributed to the shortest Tb^{III}–Eu^{III} ion distance, 0.703 nm, considered too large for effective interaction between lanthanide ions. Theoretical calculations of Tb^{III}-Eu^{III} energy transfer rates reinforce this, with the main pathway Tb^{III} [$^5D_4 \rightarrow {}^7F_5$] → Eu^{III} [$^7F_1 \rightarrow {}^5D_1$] dominated by the quadrupole–quadrupole mechanism. The Tb^{III}-Eu^{III} energy transfer resulted in lower rates compared to the ligand-to-Ln^{III} interactions, which exhibit rates orders of magnitude higher.

Declaration of competing interest

The authors declare that they have no known competing financial interests or personal relationships that could have appeared to influence the work reported in this paper.

Acknowledgements

ES, JM, JPO, JMA, PF and AV acknowledge financial support from FONDECYT 1200033 grant. JPO thanks the National Doctoral

Scholarship No. 21192195. This study was financed in part by the Brazilian agencies, Conselho Nacional de Desenvolvimento Científico e Tecnológico (CNPq, 427164/2018–4), and Fundação de Amparo à Pesquisa do Estado de Goiás (FAPEG). RCS thanks the CNPq research fellowship 310307/2021–0. This work was developed within the scope of the project CICECO-Aveiro Institute of Materials (UIDB/50011/2020, UIDP/50011/2020 & LA/P/0006/2020). ANCN thanks the LogicALL (PTDC/CTMCTM/0340/2021) project, financed by Portuguese funds through the FCT/MEC (PIDDAC).

Appendix A. Supplementary data

Supplementary data to this article can be found online at https://doi.org/10.1016/j.jre.2024.06.036.

References

1. Tang Y, Wu H, Cao W, Cui Y, Qian G. Luminescent metal–organic frameworks for white LEDs. *Adv Opt Mater*. 2021;9(23):2001817.
2. Zhao Y, Wang X, Zhang Y, Li Y, Yao X. Optical temperature sensing of up-conversion luminescent materials: Fundamentals and progress. *J Alloys Compd*. 2020;817:152691.
3. Zhang H, Shan X, Zhou L, Lin P, Li R, Ma E, et al. Full-colour fluorescent materials based on mixed-lanthanide(III) metal-organic complexes with high-efficiency white light emission. *J Mater Chem C*. 2013;1(5):888.
4. Ramya AR, Varughese S, Reddy MLP. Tunable white-light emission from mixed lanthanide (Eu^{3+}, Gd^{3+}, Tb^{3+}) coordination polymers derived from 4-(dipyridin-2-yl)aminobenzoate. *Dalton Trans*. 2014;43(28):10940.
5. Wei M, Luo L, Cui R, Wang X, Chen J, Cai Z, et al. Highly luminescent and stable lanthanide coordination polymers based 2-(3′,4′-dicarboxyphenoxy)-benzoic acid: crystal structure, photoluminescence, white light emission and fluorescence sensing. *Dyes Pigments*. 2022;206:110650.
6. Xue J, Wang Y, Yang G, Wang Y. Energy transfer, anticounterfeiting, white light emission and sensing in fine-regulating series of lanthanide metal-organic frameworks. *J Rare Earths*. 2024;42(3):446.
7. Hasegawa Y, Nakanishi T. Luminescent lanthanide coordination polymers for photonic applications. *RSC Adv*. 2015;5(1):338.
8. Ramya AR, Sharma D, Natarajan S, Reddy MLP. Highly luminescent and thermally stable lanthanide coordination polymers designed from 4-(Dipyridin-2-yl)aminobenzoate: efficient energy transfer from Tb^{3+} to Eu^{3+} in a mixed lanthanide coordination compound. *Inorg Chem*. 2012;51(16):8818.
9. Monteiro JHSK, de Bettencourt-Dias A. Lanthanide ion emission in multicolor OLEDs (Ce^{3+}, Pr^{3+}, Tb^{3+}, Dy^{3+}, Tm^{3+}, and white light Eu^{3+}/Tb^{3+} hybrid systems) and device characterization. In: *Lanthanide-based multifunctional materials*. Elsevier; 2018.
10. Chen Z, Ho C, Wang L, Wong W. Single-Molecular white-light emitters and their potential WOLED applications. *Adv Mater*. 2020;32(11):1903269.
11. Li Q, Qian J, Zhou J, Du L, Zhao Q. Highly chemically and thermally stable lanthanide coordination polymers for luminescent probes and white light emitting diodes. *CrystEngComm*. 2020;22(15):2667.
12. de Bettencourt-Dias A. Lanthanide-based emitting materials in light-emitting diodes. *Dalton Trans*. 2007;(22):2229.
13. Balashova TV, Polyakova SK, Ilichev VA, Kukinov AA, Rumyantcev RV, Fukin GK, et al. New luminescent 10-oxybenzoquinolate complexes of rare earth metals. *J Rare Earths*. 2023;41(8):1135.
14. Zhao L, Han Y, Guo G, Bai H, Wang Z, Jing H, et al. Application of three Ln(III)-coordination polymers in fields of luminescence, antibacteria and detection of Fe^{3+} and 4-nitrophenol. *J Rare Earths*. 2023;41(9):1392.
15. SeethaLekshmi S, Ramya AR, Reddy MLP, Varughese S. Lanthanide complex-derived white-light emitting solids: a survey on design strategies. *J Photochem Photobiol C Photochem Rev*. 2017;33:109.
16. Chen H-J, Chen L-Q, Lin L-R, Long L-S, Zheng L-S. Doped luminescent lanthanide coordination polymers exhibiting both white-light emission and thermal sensitivity. *Inorg Chem*. 2021;60(10):6986.
17. Rao X, Huang Q, Yang X, et al. Color tunable and white light emitting Tb^{3+} and Eu^{3+} doped lanthanide metal–organic framework materials. *J Mater Chem*. 2012;22(7):3210.
18. Krishnaraj C, Kaczmarek AM, Jena HS, Leus K, Chaoui N, Schmidt J, et al. Triggering white-light emission in a 2D imine covalent organic framework through lanthanide augmentation. *ACS Appl Mater Interfaces*. 2019;11(30):27343.
19. Yip Y-W, Wen H, Wong W-T, Tanner PA, Wong K-L. Increased antenna effect of the lanthanide complexes by control of a number of terdentate N-donor pyridine ligands. *Inorg Chem*. 2012;51(13):7013.
20. Sabbatini N, Perathoner S, Balzani V, Alpha B, Lehn J-M. Antenna effect in Eu^{3+} and Tb^{3+} cryptates. In: *Supramolecular photochemistry*. Amsterdam: Springer; 1987.
21. Hasegawa Y, Kitagawa Y. Luminescent lanthanide coordination polymers with transformative energy transfer processes for physical and chemical sensing applications. *J Photochem Photobiol C Photochem Rev*. 2022;51:100485.
22. Liu G, Lu Y-K, Ma Y-Y, Wang X-Q, Hou L, Wang Y-Y. Syntheses of three new isostructural lanthanide coordination polymers with tunable emission colours through bimetallic doping, and their luminescence sensing properties. *Dalton Trans*. 2019;48(36):13607.
23. Ma ML, Ji C, Zang SQ. Syntheses, structures, tunable emission and white light emitting Eu^{3+} and Tb^{3+} doped lanthanide metal-organic framework materials. *Dalton Trans*. 2013;42(29):10579.
24. An R, Zhao H, Hu H-M, Wang X, Yang M-L, Xue G. Synthesis, structure, white-light emission, and temperature recognition properties of Eu/Tb mixed coordination polymers. *Inorg Chem*. 2016;55(2):871.
25. Ruan J-X, Yu Y-H, Liu Y-F, Wu G, Gao J-S, Ma D-S. pH-dependant synthesis, structures and luminescent properties of a series of novel lanthanide phosphonate coordination polymers. *Polyhedron*. 2019;163:114.
26. Kang H, Peng J, Zhang Z, Zhou W. Fluorescent strengthening effect of co-doped inert rare earth ions (La^{3+}, Gd^{3+}, Lu^{3+}) on white-light-emitting of Eu–Tb(btc) coordination polymers. *J Lumin*. 2022;247:118904.
27. Chu Z-L, Zhu H-B, Hu D-H, Huang W, Gou S-H. 1D looped chain, 1D tube-like chain, and 3D inorganic–organic hybrid coordination polymers assembled from 1,6-Di(triazole-1-yl-methyl)-4-R-phenol and cadmium(II) thiocyanate. *Cryst Growth Des*. 2008;8(5):1599.
28. Zhu H, Huang C, Huang W, Gou S. A novel coordination polymer constructed from 1D neutral chains via inter-chain π–π stacking and hydrogen bonding. *Inorg Chem Commun*. 2004;7(10):1095.
29. Wyman C, Sloan P-P, Shirley P. Simple analytic approximations to the CIE XYZ color matching functions. *J Comput Graph Tech*. 2013;2(2):1.
30. McCamy CS. Correlated color temperature as an explicit function of chromaticity coordinates. *Color Res Appl*. 1992;17(2):142.
31. Kushida T. Energy transfer and cooperative optical transitions in rare-earth doped inorganic materials. I. Transition probability calculation. *J Phys Soc Japan*. 1973;34(5):1318.
32. Malta OL. Mechanisms of non-radiative energy transfer involving lanthanide ions revisited. *J Non-Cryst Solids*. 2008;354(42–44):4770.
33. Carneiro Neto AN, Moura JrRT, Shyichuk A, Paterlini V, Piccinelli F, Bettinelli M, et al. Theoretical and experimental investigation of the $Tb^{3+} \rightarrow Eu^{3+}$ energy transfer mechanisms in cubic $A_3Tb_{0.90}Eu_{0.10}(PO_4)_3$ (A = Sr, Ba) materials. *J Phys Chem C*. 2020;124(18):10105.
34. Carneiro Neto AN, Moura JrRT, Coelho JAA, E Silva-Junior M, Costa JL, Malta OL, et al. A tutorial review on the nonradiative energy transfer rates between lanthanide ions. *Chin J Lumin*. 2022;43(12):20.
35. Carneiro Neto AN, Moura RT, Malta OL. On the mechanisms of non-radiative energy transfer between lanthanide ions: centrosymmetric systems. *J Lumin*. 2019;210:342.
36. Carneiro Neto AN, Moura JrRT. Overlap integrals and excitation energies calculations in trivalent lanthanides 4f orbitals in pairs Ln-L (L = Ln, N, O, F, P, S, Cl, Se, Br, and I). *Chem Phys Lett*. 2020;757:137884.
37. Dexter DL. A theory of sensitized luminescence in solids. *J Chem Phys*. 1953;21(5):836.
38. Tanner PA, Chua M, Reid MF. Energy transfer by magnetic dipole—magnetic dipole interaction. *Chem Phys Lett*. 1993;209(5–6):539.
39. Tanner PA, Chua M, Reid MF. Energy transfer between lanthanide ions in elpasolite lattices. *J Alloys Compd*. 1995;225(1–2):20.
40. Trannoy V, Carneiro Neto AN, Brites CDS, Carlos LD, Serier-Brault H. Engineering of mixed Eu^{3+}/Tb^{3+} metal-organic frameworks luminescent thermometers with tunable sensitivity. *Adv Opt Mater*. 2021;9(6):2001938.
41. Manzur J, Fuentealba P, Gil Y, Pérez-Obando J, Morales Alfaro J, Vega Carvallo AI, et al. Tuning the emission of homometallic Dy^{III}, Tb^{III}, and Eu^{III} 1-D coordination polymers with 2,6-di(1H-1,2,4-triazole-1-yl-methyl)-4-R-phenoxo ligands: sensitization through the singlet state. *Inorg Chem*. 2023;62(47):19195.
42. Zhang Z, He Y-N, Liu L, Lü XQ, Zhu XJ, Wong W-K, et al. Pure white-light and colour-tuning of Eu^{3+}–Gd^{3+}-containing metallopolymer. *Chem Commun*. 2016;52(18):3713.
43. te Kulve M, Schlangen L, Schellen L, Souman JL, van Marken Lichtenbelt W. Correlated colour temperature of morning light influences alertness and body temperature. *Physiol Behav*. 2018;185:1.
44. Wei Y, Sa R, Li Q, Wu K. Highly stable and sensitive LnMOF ratiometric thermometers constructed with mixed ligands. *Dalton Trans*. 2015;44(7):3067.
45. Fomina IG, Dobrokhotova ZV, Aleksandrov GG, Zhilov VI, Malkerova IP, Alikhanyan AS, et al. Synthesis and characterization of new heterodinuclear (Eu, Tb) lanthanide pivalates. *Polyhedron*. 2013;50(1):297.
46. Carneiro Neto AN, Mamontova E, Botas AMP, Brites CDS, Ferreira RAS, Rouquette J, et al. Rationalizing the thermal response of dual-center molecular thermometers: the example of an Eu/Tb coordination complex. *Adv Opt Mater*. 2022;10(5):2101870.

47. Lyubov DM, Carneiro Neto AN, Fayoumi A, Lyssenko KA, Korshunov VM, Taydakov IV, et al. Employing three-blade propeller lanthanide complexes as molecular luminescent thermometers: study of temperature sensing through a concerted experimental/theory approach. *J Mater Chem C*. 2022;10(18):7176.
48. Paulose PI, Jose G, Thomas V, Unnikrishnan NV, Warrier MKR. Sensitized fluorescence of Ce^{3+}/Mn^{2+} system in phosphate glass. *J Phys Chem Solid*. 2003;64(5):841.
49. Fairley M, Livera MMVS, Chen W, et al. Metal–organic frameworks of lanthanide iminodiacetates and tartrates: synthesis, structural characterization and luminescence properties — Commemorating the 100th anniversary of the birth of Academician Guangxian Xu. *J Rare Earths*. 2021;39(5):487.